ISPRS Journal of Photogrammetry and Remote Sensing 114 (2016) 125–136

Contents lists available at ScienceDirect

ISPRS Journal of Photogrammetry and Remote Sensing

journal homepage: www.elsevier.com/locate/isprsjprs

Combined adjustment of multi-resolution satellite imagery for improved geo-positioning accuracy

Shengjun Tang [a,b,c], Bo Wu [a,*], Qing Zhu [b,c,d]

[a] Department of Land Surveying and Geo-Informatics, Hong Kong Polytechnic University, Hung Hom, Kowloon, Hong Kong
[b] State Key Laboratory of Information Engineering in Surveying Mapping and Remote Sensing, Wuhan University, Wuhan, PR China
[c] Faculty of Geosciences and Environmental Engineering, Southwest Jiaotong University, Chengdu, PR China
[d] Collaborative Innovation Center for Geospatial Technology, 129 Luoyu Road, Wuhan, PR China

ARTICLE INFO

Article history:
Received 23 November 2015
Received in revised form 10 February 2016
Accepted 10 February 2016

Keywords:
Satellite imagery
Combined adjustment
Geo-positioning accuracy
Multiple resolution

ABSTRACT

Due to the widespread availability of satellite imagery nowadays, it is common for regions to be covered by satellite imagery from multiple sources with multiple resolutions. This paper presents a combined adjustment approach to integrate multi-source multi-resolution satellite imagery for improved geo-positioning accuracy without the use of ground control points (GCPs). Instead of using all the rational polynomial coefficients (RPCs) of images for processing, only those dominating the geo-positioning accuracy are used in the combined adjustment. They, together with tie points identified in the images, are used as observations in the adjustment model. Proper weights are determined for each observation, and ridge parameters are determined for better convergence of the adjustment solution. The outputs from the combined adjustment are the improved dominating RPCs of images, from which improved geo-positioning accuracy can be obtained. Experiments using ZY-3, SPOT-7 and Pleiades-1 imagery in Hong Kong, and Cartosat-1 and Worldview-1 imagery in Catalonia, Spain demonstrate that the proposed method is able to effectively improve the geo-positioning accuracy of satellite images. The combined adjustment approach offers an alternative method to improve geo-positioning accuracy of satellite images. The approach enables the integration of multi-source and multi-resolution satellite imagery for generating more precise and consistent 3D spatial information, which permits the comparative and synergistic use of multi-resolution satellite images from multiple sources.

1. Introduction

Due to its advantages of high resolution, short revisit time and relatively low cost, satellite imagery has been widely used in a variety of fields to derive 3D spatial information for purposes such as cartographic mapping (Wang et al., 2014), modeling buildings (Baltsavias et al., 2001; Fraser et al., 2002), mapping coastlines (Di et al., 2003a) or monitoring disasters (Glenn et al., 2006; Kasai et al., 2009). The satellites launched in recent years offer multiple spatial resolutions, e.g., ranging from 3.5 m/pixel for the Chinese ZY-3 imagery (Wang et al., 2014) to 1.5 m/pixel for the SPOT-7 imagery, to the approximately half-meter-level resolution of the Pleiades-1, GeoEye-1 or Worldview-1 imagery (Croft, 2008; Poli et al., 2013).

The obtainable geo-positioning accuracy of satellite images is highly relevant to factors such as spatial resolution and imaging geometry (Li et al., 2008; Fraser and Hanley, 2003; Di et al., 2003b). Previous studies have revealed that different types of satellite imagery have various levels of geo-positioning errors if they rely entirely on the rational polynomial coefficients (RPCs) provided by the vendors. For example, a horizontal error of about 15 m was found for the ZY-3 stereo imagery (Pan et al., 2013). The GeoEye-1 imagery also has a geolocation error range of about 3 m (CE90) (Fraser and Ravanbakhsh, 2009). Similar findings have been reported for other types of satellite imagery, such as a horizontal error of 16–25 m for the IKONOS "Geo" product (Dial and Grodecki, 2002) or a horizontal error of 23 m and a vertical error of 17 m for the QuickBird "Basic Level" imagery (Qiao et al., 2010). Traditional methods for obtaining improved geo-positioning accuracy from satellite images rely on using a number of ground control points (GCPs) to compensate for bias through mathematic functions such as translations, affines or polynomial models (Toutin, 2006; Li et al., 2008; Fraser and Hanley, 2005).

* Corresponding author. Tel.: +852 2766 4335; fax: +852 2330 2994.
E-mail address: bo.wu@polyu.edu.hk (B. Wu).

http://dx.doi.org/10.1016/j.isprsjprs.2016.02.003
0924-2716/

With the widespread availability of satellite imagery, it is increasingly common for the same region to be covered by multiple satellite images from different sources with different resolutions. This situation presents a significant opportunity for the integrated processing of these multi-source multi-resolution satellite images. Such integrated processing can allow satellite images with lower geo-positioning accuracy to be improved with the aid of images having higher geo-positioning accuracy, so that inconsistencies in the derived 3D spatial information can be reduced.

Several studies have focused on the geometric integration of different types of images for improved geo-positioning accuracy. For example, based on the rational function model, Niu et al. (2005) investigated the integration of IKONOS and QuickBird images. They compared the geo-positioning accuracies of the different combinations from these images with different convergent angles. Li et al. (2008) presented another approach to improve the geo-positioning accuracy of IKONOS and QuickBird imagery by using aerial images acquired over the same region of Tampa Bay, Florida. Tong et al. (2010a) presented a similar study to improve QuickBird's geo-positioning accuracy by integrating aerial images and QuickBird imagery covering the same region in Shanghai, China. Jeong et al. (2015) investigated the positioning accuracy of image pairs achieved by integrating images from multiple satellites, including IKONOS, QuickBird, and KOMPSAT-2 imagery for Daejeon, Korea. From single-satellite stereo pairs to multiple-satellite image pairs, all available combinations were examined with a rational function model. The results from these studies demonstrate that the integration of images from multiple satellites is able to improve the geo-positioning accuracy of satellite images. However, the methods for geometric integration of multi-source and multi-resolution imagery used in these studies actually present a space intersection of images, with an antecedent step for compensating the bias in the RPCs of the satellite images through a shift or an affine transformation. This integration strategy is rather ad hoc, and the methods still require a number of high-quality GCPs for the integrated processing to work. In addition, previous methods didn't systematically investigate the image RPCs dominating the geo-positioning accuracy and the solutions for over-parameterization problems in the integration process.

This paper presents an approach for the geometric integration of multi-source multi-resolution satellite imagery through combined adjustment that achieves improved geo-positioning accuracy without the use of GCPs. Section 2 presents a literature review on the various methods for improving the geo-positioning accuracy of satellite images. The details of the combined adjustment approach for the geometric integration of multi-source multi-resolution satellite imagery are provided in Section 3. Section 4 reports the experimental analyses using a set of ZY-3, SPOT-7 and Pleisdes-1 imagery in Hong Kong, and a set of Cartosat-1 and Worldview-1 imagery in Catalonia, Spain. Finally, concluding remarks are presented and discussed in Section 5.

2. Literature review

The rigorous physical model (RPM) and the rational function model (RFM) are the two main sensor models to describe the geometrical relationships between image points and their corresponding ground points in satellite imagery (Fraser, 1999; Tao and Hu, 2001; Dial and Grodecki, 2002). However, the RPMs for commercial satellite imagery may not be computationally efficient due to their complexity, and may not even be available to general users (Fraser et al., 2006; Habib et al., 2007). Instead, the RFMs are provided by the image vendors. RFMs have served as alternative sensor models and have been widely used to derive 3D spatial information from various types of satellite images. The following equation is an example of an RFM based on third-order polynomials:

$$l = \frac{N_1(P,L,H)}{N_2(P,L,H)} = \frac{(1PLH\ldots LH^2H^3)(a_1a_2a_3a_4\ldots a_{19}a_{20})^T}{(1PLH\ldots LH^2H^3)(b_1b_2b_3b_4\ldots b_{19}b_{20})^T}$$
$$s = \frac{N_3(P,L,H)}{N_4(P,L,H)} = \frac{(1PLH\ldots LH^2H^3)(c_1c_2c_3c_4\ldots c_{19}c_{20})^T}{(1PLH\ldots LH^2H^3)(d_1d_2d_3d_4\ldots d_{19}d_{20})^T} \quad (1)$$

where (l, s) are the image coordinates and (P, L, H) are the object coordinates (latitude, longitude and height) in a geographic reference system. Third-order polynomials usually consist of 78 rational polynomial coefficients (RPCs), including a_i, b_i, c_i and d_i $(i = 1–20)$ (b_1 and d_1 are equal to 1). For each image, the RPCs are normally provided as metadata files by the image supplier (Habib et al., 2007; Li et al., 2008).

For a stereo pair of satellite images, the 3D ground coordinates of points on the stereo imagery can be calculated through a space intersection using the RPCs of each image. Usually, there are discrepancies between the 3D ground coordinates as directly derived from the RPCs and the true coordinates. These discrepancies are considered as degrees of geo-positioning accuracy. As mentioned previously, different satellite imagery have different levels of geo-positioning accuracy. Traditional methods to improve the geo-positioning accuracy of satellite images simply use GCPs to compensate the bias in RPCs through mathematical functions. For example, Di et al. (2003b) used a 3D affine transformation model to compensate for the discrepancies in object space and to refine the RPC-derived ground coordinates of IKONOS images. An accuracy of 1.5 m in planimetry and 1.6 m in height was achieved through this approach. Wang et al. (2005) compared the results from different bias-correction models, including translation, scale and translation, affine and second-order polynomial models using IKONOS and QuickBird imagery. It was found that meter-level accuracy can be obtained using an appropriate model and a number of good quality GCPs. Similar results have been reported for other types of satellite images (Fraser and Hanley, 2005; Toutin, 2006; Habib et al., 2007; Fraser and Ravanbakhsh, 2009).

Instead of adding corrections to image spaces or to object space, Tong et al. (2010a) proposed a method to directly modify and regenerate the 78 RPCs based on bias-correction models. They tested the method using a stereo pair of QuickBird images of Shanghai, China. The results indicated that sub-meter-level accuracy can be achieved using a sufficient number of GCPs with appropriate distributions. This method allows the convenient use of satellite images for mapping applications. The regenerated RPCs can be directly used as inputs in commercial photogrammetric software systems without pre-processing. However, their method also requires a considerable number of GCPs to ensure the solution converged.

Due to the widespread availability of satellite imagery from different sources in recent years, researchers have begun to investigate the integration of multi-source, multi-resolution imagery for improved geo-positioning accuracy. Li et al. (2008) compared 3D geo-positioning accuracies from different combinations of IKONOS and QuickBird images covering the same region. Their results indicated that the geo-positioning accuracy of satellite images is related to the spatial resolution and the convergence angle of the stereo images. Their results also showed that the integration of higher resolution QuickBird images with IKONOS images produced better geo-positioning accuracy than the integration of an IKONOS pair. Li et al. (2008) also investigated the achievable accuracy by integrating satellite images with aerial images, and found that the geo-positioning accuracy from a stereo pair of IKONOS or QuickBird images could be improved to about 0.3 m in horizontal and 0.4 m in height by integrating a set of aerial images, or even just a single aerial image (Li et al., 2008). Similar results have been reported by Tong et al. (2010b) in using combinations of aerial images and QuickBird images covering the same region. However,

the above-mentioned methods still require GCPs to compensate for the bias in the RPCs of satellite images, and then integrating satellite images from different sources, or satellite images with aerial images for improved geo-positioning accuracy through space intersections.

This paper presents an approach to geometric integration of multi-source multi-resolution satellite imagery through a strict combined adjustment model for improved geo-positioning accuracy. Compared with previous studies, this approach has the following merits. First, the RPCs of the satellite images are directly adjusted and improved through the combined adjustment, so that they can be directly used in commercial photogrammetric software systems for further applications. Second, only the RPCs that are dominant in geo-positioning accuracy rather than the full set of RPCs are used in the combined adjustment. Therefore, the possible over-parameterization problems that lead to unstable solutions are alleviated. Third, a ridge estimation strategy is introduced to improve the condition of the normal equation in the adjustment model and to further ensure a converged solution of the combined adjustment.

3. Combined adjustment of multi-source, multi-resolution satellite imagery

3.1. Overview of the approach

The combined adjustment model is developed for the geometric integration of multi-source multi-resolution satellite imagery. The RPCs of images to be corrected (referred to as slave images) are adjusted iteratively through integration with a single or a stereo pair of satellite images, referred to as the reference image(s). The criterion for the selection of the reference image(s) is that they should have higher or greater geo-positioning accuracy than that of the slave images. Generally, the geo-positioning accuracy of satellite images can be found in literature or in the metadata provided by image vendors and, normally, satellite images with higher resolution have higher geo-positioning accuracy. Tie points are selected in the overlapping regions of the images. Due to the errors in the RPCs of images and the inconsistencies among different image sources, the ground coordinates of the tie points derived from the slave images may differ from those obtained from the reference images. The combined adjustment model is used to reduce these inconsistencies, to remove the bias in the RPCs of the images and to subsequently improve the geo-positioning accuracy.

The combined adjustment does not use all of the RPCs, only those that dominate the geo-positioning accuracy of the satellite images. We analyzed the influences of individual RPCs from satellite imagery on geo-positioning accuracy and found that the RPCs including a_1–a_5, b_1–b_5, c_1–c_5 and d_1–d_5 (18 RPCs in total, as b_1 and d_1 are equal to 1) dominate the geo-positioning accuracy. These 18 RPCs are called the dominating RPCs. Rather than using the full RPC set, we use only the dominating RPCs in the combined adjustment, thereby greatly reducing the computational complexity and guaranteeing the convergence of the mathematical solution. Further details on the determination of dominating RPCs can be found in Wu et al. (2015).

The dominating RPCs of the slave images, the tie points identified on the images and the ground coordinates of the tie points are all used as observables in the combined adjustment model. A weighting strategy is designed to assign proper weights for each type of observable in the adjustment. The L-Curve based method (Hansen and O'Leary, 1993; Neumaier, 1998) is introduced in the combined adjustment to determine the ridge parameters for better converged solutions. The combined adjustment model iteratively improves the original dominating RPCs of the slave images provided by image suppliers, based on the least-squares principle. The framework of the combined adjustment approach is shown in Fig. 1.

3.2. Combined adjustment model

The RFM Eq. (1) of satellite images can be linearized to obtain the observation equations of the combined adjustment model. These equations can be represented in matrix form as follows:

$$\begin{aligned} V_1 &= AX_1 - L_1, & P_1 \\ V_2 &= BX_2 - L_2, & P_2 \\ V_3 &= CX_1 + DX_2 + EX_3 - L_3, & P_3 \end{aligned} \tag{2}$$

The observation equation system includes the following three types of observation equations. The first and second observation equations are the pseudo observation equations for the dominating RPCs of the reference image(s) and slave images, respectively. By the term "pseudo", it means the measurements are estimated instead of real measurements (such as the precisely matched tie points) in other types of observations. X_1 and X_2 are the vectors of corrections for the dominating RPCs of the images. V_1 and V_2 are the vectors of residual errors. L_1 and L_2 are the observation vectors of the corresponding dominating RPCs. Their initial values are selected from the original RPCs provided by image vendors. The refined RPCs are assumed to fluctuate around them. It should be noted that, the dominating RPCs of the reference image(s) are also allowed to adjust as indicated by the first observation equation, which corresponds to the case when additional GCPs are available (noted that the adjustment model requires no GCPs to work) and they can be used to improve the dominating RPCs of the reference image(s) in the combined adjustment. Otherwise, the dominating RPCs of the reference image(s) will not change during the combined adjustment by giving them infinite weights. For the second observation equation, more than one observation equations of this type can be constructed if more than one types of satellite images involved for correction. In this case, different weights can be assigned to each of the observation equation.

The third observation equation corresponds to the tie points identified from the images. They connect the 3D ground points and their image measurements by the RPCs of the images as indicated in Eq. (1). X_3 is the vector of corrections to the ground coordinates of the tie points. L_3 is the observation vector of the tie points. V_3 is the vector of residual errors for this observation equation.

In the observation equations, P_1, P_2 and P_3 are the weights of the corresponding observation equations. The determination of weights is detailed in Section 3.4. The coefficient matrices A, B, C, D, and E contain the partial derivatives of the parameters to be corrected in each observation equation. A ridge parameter is calculated to improve the condition number of the design matrix, and the equations are solved iteratively based on a least-squares method to obtain a convergent solution.

3.3. Determination of tie points

Tie points, identified in the multi-source multi-resolution satellite imagery, are necessary for the combined adjustment. There are two steps in determining the tie points. In the first step, the satellite images with higher resolution are down-sampled to be the same resolution with the images with lower resolution. A self-adaptive, triangulation-constrained image matching (SATM) method (Wu et al., 2011a, 2012; Zhu et al., 2007) is employed to automatically obtain a large number of corresponding feature points (homogeneous points that represent the same texture) from the satellite images. The main steps of SATM are: (1) Several robust

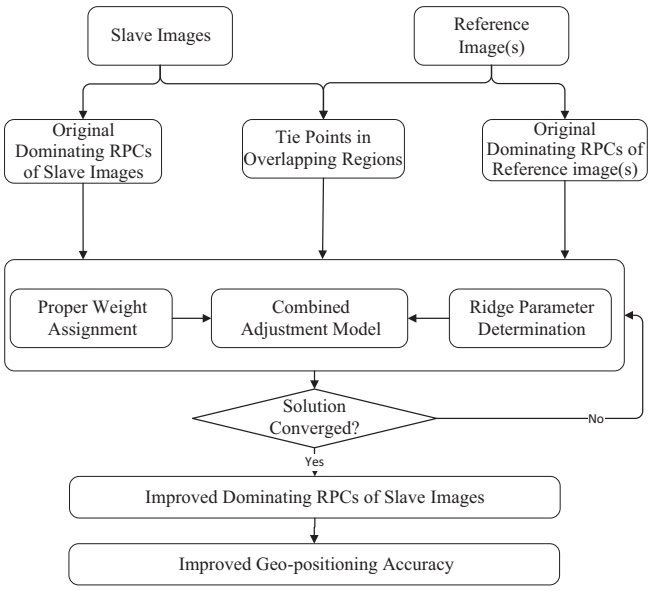

Fig. 1. Framework of the combined adjustment approach for multi-source multi-resolution satellite imagery.

seed points automatically obtained are used to generate a pair of initial corresponding Delaunay triangulations covering the overlapping region the images; (2) feature points are matched within each pair of the corresponding triangles by cross-correlating with the intensities; and (3) the newly matched points are inserted into the triangulations, which are updated dynamically. As the most distinctive point is always successfully matched first, the dynamic updating of triangulations adapts automatically to image textures, and ultimately produces more reliable matching results (Wu et al., 2011a, 2012). The matched points from SATM are then projected to the satellite images with their original resolutions. In the second step, an interactive process is carried out to manually select robust tie points from the matched points from the previous step. These tie points should be evenly distributed on the satellite images.

It should be noted that due to the variations in viewing perspective, the points identified from the reference image with higher resolution may not always be visible in the slave images. As shown in Fig. 2, the black points marked on the reference image can be used as tie points. The gray points on the reference image are regarded as invalid, because homogeneous points representing the same texture cannot be identified from the slave image. The matched tie points are checked carefully and possible unreliable points are eliminated manually. Normally, the combined adjustment requires dozens of tie points with favorable reliability and distribution throughout the overlapping region of the multi-source images.

3.4. Weight determination

In the combined adjustment model of Eq. (2), the weights P_1, P_2, and P_3 represent the respective contribution of the observations in the adjustment process. In this investigation, the weights are determined as follows.

For P_1 and P_2 representing the weights for the dominating RPCs of the reference image(s) and slave images, the information on the accuracy of the original RPCs is not provided in the vender-supplied metafile. As this investigation emphasizes combined adjustment of multi-source satellite images requiring no GCPs, the reference image(s) will be used as an absolute control and infinite weights will be assigned to P_1 as mentioned previously. The accuracies of slave images can be estimated by comparing the ground coordinates of tie points derived from them with those from the reference images through space intersection using the original RPCs. The weight P_2 can be set as $1/(\sigma_P^2 + \sigma_L^2 + \sigma_H^2)$, of which σ_P, σ_L and σ_H are the aforementioned comparison results in three directions. In cases when GCPs are available, P_1 can be determined similar to P_2, just in this case the comparison is between the ground coordinates derived from the original RPCs and the GCPs. This strategy ensures that the images with higher accuracy are endowed with greater weights, and therefore contribute more in the combined adjustment process.

For the weight P_3 related to the tie points, one third of a pixel is chosen, as this is the paradigm in determining the pixel measurement error for tie point observations. On the basis of photogrammetry studies (Yoon and Shan, 2005; Wu et al., 2011b, 2014), moderate changes are permitted in the weight magnitude during the combined adjustment process. The above strategies provide a basic guide for determining an optimum weight for each observation. More than one test may need to be conducted to estimate the best weights in practice.

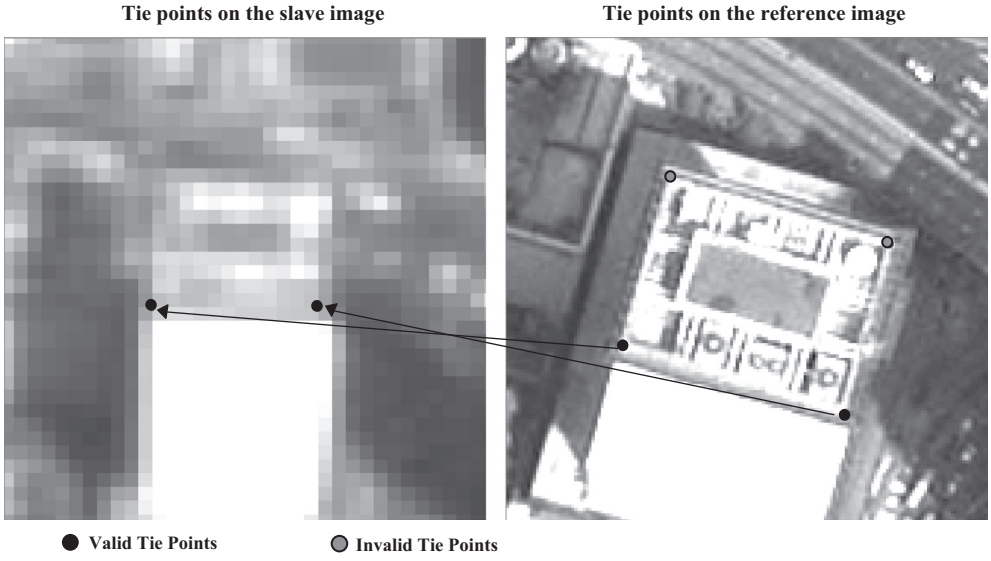

Fig. 2. Determination of tie points in multi-source multi-resolution satellite imagery.

Table 1
Parameters of the satellite imagery used in the experiments.

Items	ZY-3 imagery		SPOT-7 imagery		Pleiades-1 imagery	
	Forward-looking	Backward-looking	Forward-looking	Backward-looking	Forward-looking	Backward-looking
Acquisition date and time	2013/3/8 11:11	2013/3/8 11:12	2014/12/9 7:33	2014/12/9 7:03	2013/3/4 2:31	2013/3/4 2:30
Image size (pixels)	16,306 × 16,384	16,306 × 16,384	6833 × 5297	6833 × 5297	15,173 × 20,542	15,374 × 20,628
Resolution (m/pixel)	3.368	3.379	1.799	1.874	0.504	0.502
Convergence angle (°)	44		60		14.8	

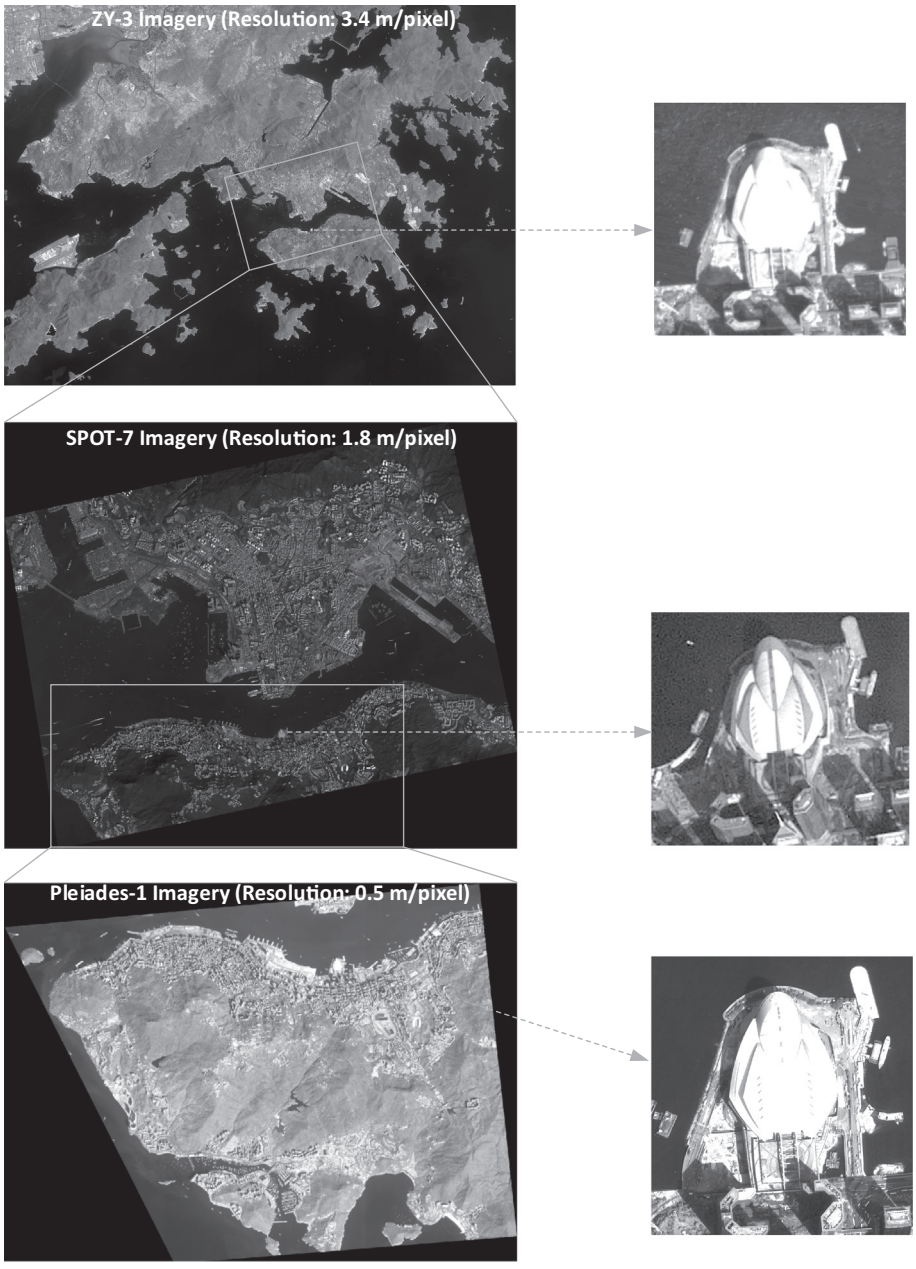

Fig. 3. The ZY-3, SPOT-7 and Pleiades-1 imagery in Hong Kong showing different levels of coverage and resolution, with zoom-in images of the Hong Kong Convention and Exhibition Center from each image source showing in the right.

3.5. Ridge parameter determination

In the combined adjustment model, the values of the denominators in the error equation are highly dependent on the distribution of the tie points (Tao and Hu, 2001). Moreover, Fraser and Yamakawa (2004) pointed out that the RFM model with 78 RPCs might be over-parameterized, and the problem of ill-conditioned normal equations can easily occur when calculating the solutions. Traditional least-squares adjustment cannot obtain a convergent solution. In this research, ridge estimation is introduced to improve the condition of the normal equation and to ensure a converged solution of the combined adjustment. The determination of the ridge parameter is important in ridge estimation. Wang and Ou (2004) and Yuan and Lin (2008) compared different methods for

ridge estimation including the L-Curve method, the ridge mark method, and the generalized cross-validation method. Both the two investigations draw a conclusion that the L-Curve method is the most reliable and valid one for determining the ridge parameter. Details of the ridge parameter determination are described below.

After rewriting Eq. (2), the observation error equation of the combined adjustment model can be formed as:

$$V = DX - L, P_1, P_2, P_3 \tag{3}$$

where

$$D = \begin{bmatrix} A & 0 & 0 \\ 0 & B & 0 \\ C & D & E \end{bmatrix}, \; X = \begin{bmatrix} X_1 \\ X_2 \\ X_3 \end{bmatrix}, \; L = \begin{bmatrix} L_1 \\ L_2 \\ L_3 \end{bmatrix}.$$

The direct solution of the RPCs and the ground coordinates of tie points can be represented as:

$$\begin{bmatrix} X_1 \\ X_2 \\ X_3 \end{bmatrix} = \left(\begin{bmatrix} P_1A & 0 & 0 \\ 0 & P_2B & 0 \\ P_3C & P_3D & P_3E \end{bmatrix}^T \cdot \begin{bmatrix} P_1A & 0 & 0 \\ 0 & P_2B & 0 \\ P_3C & P_3D & P_3E \end{bmatrix} + kU \right)^{-1} \cdot \begin{bmatrix} P_1A & 0 & 0 \\ 0 & P_2B & 0 \\ P_3C & P_3D & P_3E \end{bmatrix}^T \cdot \begin{bmatrix} P_1L_1 \\ P_2L_2 \\ P_3L_3 \end{bmatrix} \tag{4}$$

where k is the ridge parameter, and U is the unit matrix.

According to the L-Curve method (Hansen and O'Leary, 1993; Neumaier, 1998), a fitting curve of k can be obtained as follows:

$$(\alpha(k), \beta(k)) = (\log ||DX - L||_k, \; \log ||X||_k) \tag{5}$$

where $\log||DX - L||$ and $\log||X||$ serve as the X-axis and Y-axis, respectively. The quasi-optimal k value can be determined when the fitting curve has the maximum curvature, and this value can then be used in Eq. (4) to obtain a converged solution of the combined adjustment.

4. Experimental analysis

4.1. Experiment using multi-resolution satellite imagery in Hong Kong

4.1.1. Used data

Multi-source multi-resolution satellite images including ZY-3, SPOT-7 and Pleiades-1 panchromatic images of Hong Kong were used for systematic experimental analysis. The ZY-3 and Pleiades-1 images were taken in March 2013. The SPOT-7 imagery was taken in December 2014. The ZY-3 imagery has the lowest resolution, of about 3.4 m/pixel, covering an area of W 113.81°–114.42° and N 22.03°–22.63°. The SPOT-7 imagery has a better resolution, of about 1.8 m/pixel, and covers an area of W 114.1°–114.23° and N 22.24°–22.37°. The Pleiades-1 imagery has the highest resolution of 0.5 m/pixel and covers an area of W 114.05°–114.26° and N 22.23°–22.30°. The detailed parameters of these three image sets are listed in Table 1. Fig. 3 shows the overview of the three image sets.

This investigation used the translation-rectified airborne LiDAR data collected in Hong Kong as ground truth data for geo-position accuracy evaluation. The airborne LiDAR data were collected between December 1, 2010 and January 8, 2011. According to the metafile of the LiDAR data, these measurements have a vertical accuracy about 10 cm and the horizontal accuracy is about 1 m. A number of traverse survey points obtained from the Lands Department of Hong Kong[1] were used to rectify the LiDAR data through a rigid transformation. The accuracies of the traverse survey points are at millimeter level, and therefore the accuracy of the LiDAR data after transformation is at the same level. For the purpose of selecting ground check points (CKPs) from the LiDAR data, the LiDAR data was firstly interpolated as a 3D surface with a resolution of 30 cm, and then the CKPs (corners of buildings) were manually selected from the reconstructed surface of LiDAR data referring to the corresponding satellite image. Different views of the 3D surface, including the view angle similar to the one of the satellite image, were examined when determining the locations of the CKPs to ensure the reliability. Fig. 4 shows an example of CKP selection. The derived ground coordinates of the CKPs were further checked by a number of GPS survey points, and the differences between them and the GPS survey points were from 0.08 to 0.2 m.

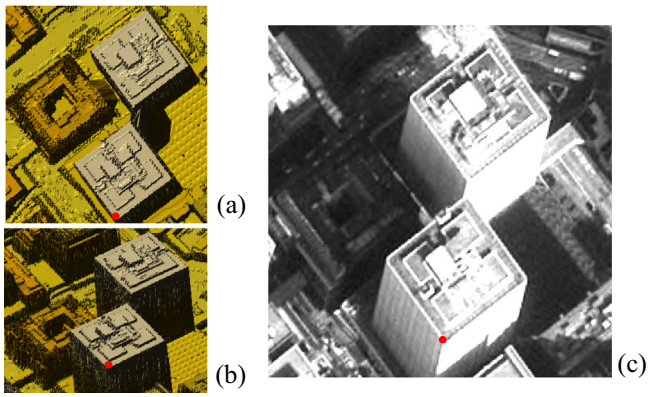

Fig. 4. Selection of CKPs (red dots) from the airborne LiDAR data referring to the satellite image. (a) 3D reconstructed surface of the LiDAR data viewing from top, (b) 3D reconstructed surface of the LiDAR data with a view angle similar to the one of the satellite image, and (c) the corresponding area in the Pleiades-1 image.

In the experimental analysis, the satellite imagery with the highest resolution, i.e., the Pleiades-1 imagery, was used as the reference imagery to correct the dominating RPCs of the ZY-3 and SPOT-7 imagery. For the combination of ZY-3 and Pleiades-1 imagery, there were 67 tie points identified on both the Pleiades-1 and ZY-3 stereo-image pairs, and 53 CKPs were selected in the overlapping region of the two image sets. For the combination of SPOT-7 and Pleiades-1 imagery, 51 tie points were identified on both the Pleiades-1 and SPOT-7 stereo-image pairs, and there were 42 CKPs selected in the overlapping region of these two image sets. The 3D coordinates of the CKPs were derived from the airborne LiDAR data after transformation as aforementioned. Fig. 5 shows the experimental overlapping area of the ZY-3, SPOT-7 and Pleiades-1 imagery, with corresponding tie points and CKPs marked on the image.

4.1.2. Performance of the combined adjustment

The tie points identified from the overlapping region of the ZY-3, SPOT-7 and Pleiades-1 imagery, and the original RPCs of these images were input into the combined adjustment model. The initial values of the ground coordinates of the tie points were obtained from a direct space intersection using the corresponding original RPCs of the respective images. After processing, we obtained the corrected dominating RPCs of the ZY-3 and SPOT-7 images. Two different experimental schemes were investigated in this research. One scheme used the stereo pair of the Pleiades-1 imagery as reference images, and the other used only a single Pleiades-1 image (either forward-looking or backward-looking) as a reference image. The same tie points and CKPs were used in both schemes.

The L-Curves for the combined adjustment of ZY-3, SPOT-7 and Pleiades-1 images are shown in Fig. 6. In the experiment, the initial value of k was set to be 10^{-10}. To obtain the optimal value of k, 150

[1] Available at http://www.geodetic.gov.hk/smo/gsi/programs/en/traverse_station.asp.

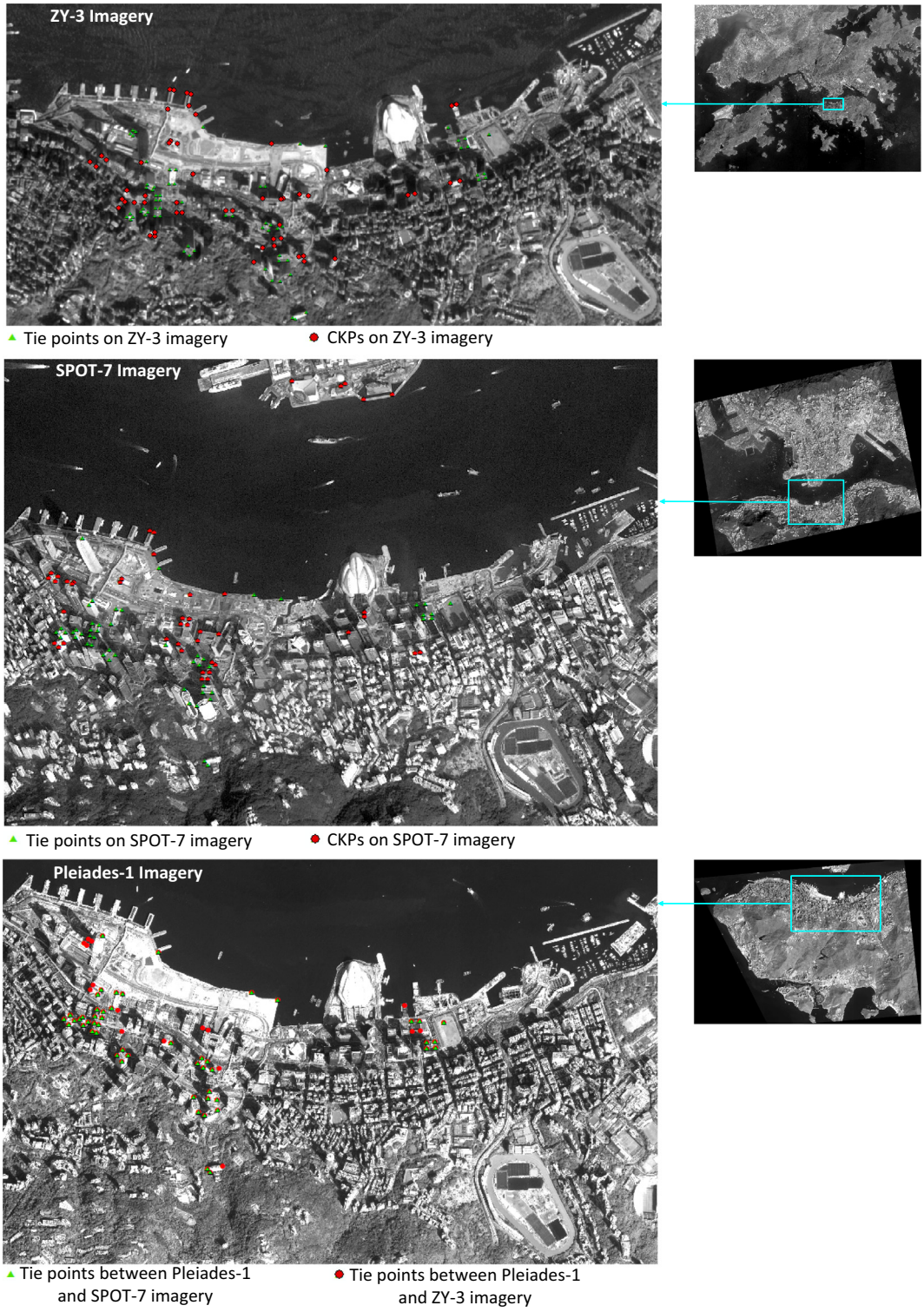

Fig. 5. The experimental overlapping area of the ZY-3, SPOT-7 and Pleiades-1 imagery, marked with the tie points and CKPs used in the experimental analysis.

sets of k were tested. The value of k in each iteration was set as $(10^{-10}) * 1.25^n$, where n is the number of iterations. Therefore, 150 sets of the values of $\log||DX - L||$ and $\log||X||$ were calculated, and fitting curves between them were generated as shown in Fig. 6. The optimal k value can be determined when the fitting curve has the maximum curvature (crosses marked in Fig. 6). The ridge parameters were determined as 0.794 for the ZY-3 image sets and 0.501 for the SPOT-7 image sets.

The performance of the combined adjustment was examined in object space. The ground coordinates of the CKPs on the ZY-3 and SPOT-7 imagery were obtained using their original RPCs (direct space intersections) and the RPCs after combined adjustment. They were compared with the ground coordinates of the CKPs derived from the translation-rectified LiDAR data to calculate the discrepancies (RMSE) in the X, Y and Z directions. To evaluate the performance of the proposed combined adjustment approach, the results

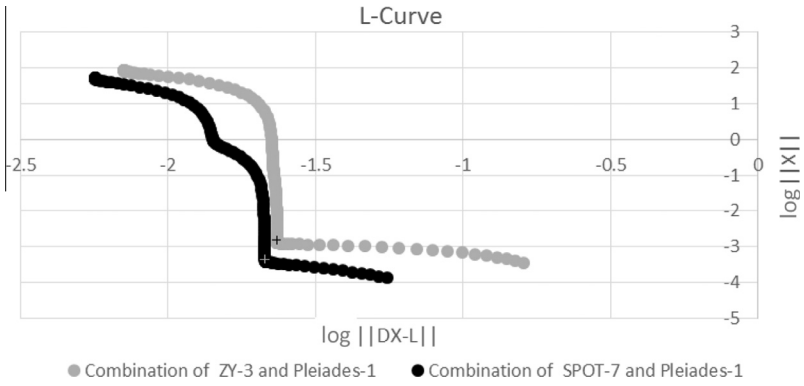

Fig. 6. L-Curves for the combined adjustment of ZY-3, SPOT-7 and Pleiades-1 imagery.

Table 2
Geo-positioning accuracies for Pleiades-1, ZY-3 and SPOT-7 imagery from different approaches.

Combinations	Methods	Geo-positioning accuracy (RMSE in meters)			Relative improvements comparing with the results of direct space intersection	
		x	*y*	*z*	Horizontal direction (%)	Vertical direction (%)
Pleiades-1(S)	Direct space intersection	1.26	1.39	1.36		
ZY-3(S)	Direct space intersection	14.42	6.80	2.87		
ZY-3(S)	Affine transformation (using 6 GCPs)	3.91	3.86	2.48	65.53	13.59
ZY-3(S) + Pleiades-1(F)	Combined adjustment	3.99	3.78	2.36	65.52	17.77
ZY-3(S) + Pleiades-1(B)	Combined adjustment	3.59	3.79	2.35	67.25	18.12
ZY-3(S) + Pleiades-1(S)	Combined adjustment	3.77	3.77	2.36	66.55	17.77
SPOT-7(S)	Direct space intersection	5.75	1.70	4.54		
SPOT-7(S)	Affine transformation (using 6 GCPs)	2.52	1.98	3.52	46.55	22.47
SPOT-7(S) + Pleiades-1(F)	Combined adjustment	2.24	2.18	3.34	47.87	26.43
SPOT-7(S) + Pleiades-1(B)	Combined adjustment	1.96	1.68	3.22	56.95	29.07
SPOT-7(S) + Pleiades-1(S)	Combined adjustment	2.02	1.70	3.28	55.97	27.75

Note: S – stereo, F – forward-looking, B – backward-looking.

were compared with traditional method of using GCPs (6 GCPs were carefully selected for each image set) to compensate the bias of RPCs through affine transformation for the ZY-3 and SPOT-7 imagery. The results are listed in Table 2.

From Table 2, the following can be noted:

(1) Through the direct space intersection using the original RPCs, the Pleiades-1 imagery produces a horizontal accuracy of 1.88 m and a vertical accuracy of 1.36 m. The ZY-3 imagery produces a horizontal accuracy of 16 m and a vertical accuracy of 2.87 m. The SPOT-7 imagery produces a horizontal accuracy of 6 m and a vertical accuracy of 4.5 m. As expected, the Pleiades-1 imagery has the best geo-positioning accuracy.

(2) The use of a single or a stereo pair of Pleiades-1 images in the combined adjustment improves the geo-positioning accuracy of the ZY-3 imagery to about 5 m in horizontal direction, and to 2.5 m for the SPOT-7 imagery in horizontal direction. The accuracies in the vertical direction for the ZY-3 and SPOT-7 imagery are also improved. The geo-positioning accuracies from the combined adjustment are

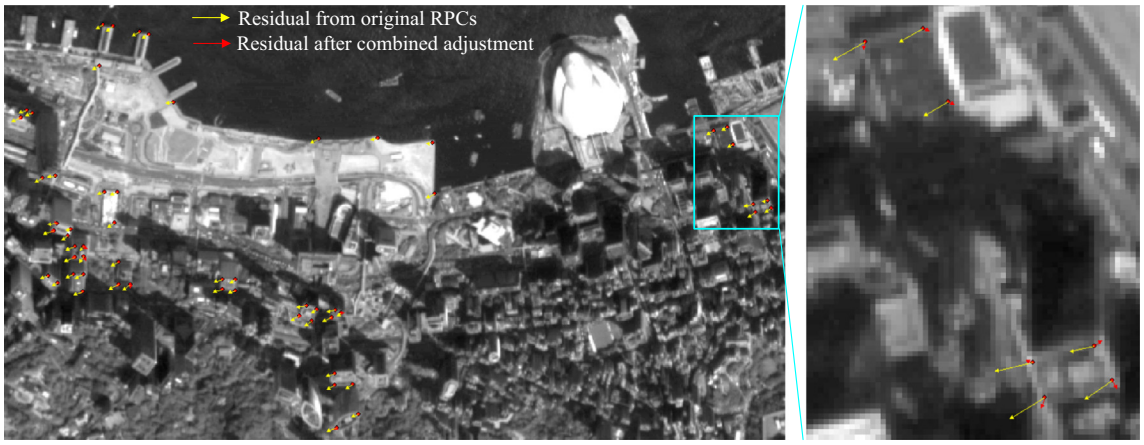

Fig. 7. Image residuals of the CKPs illustrated on the ZY-3 image.

Table 3
Statistics of the image residuals before and after combined adjustment for the image set of ZY-3 and Pleiades-1.

Methods	Residuals	MAE (pixels)	Max (pixels)	Min (pixels)
ZY-3(S) direct space intersection	Residual *X*	6.27	8.94	3.19
	Residual *Y*	2.80	5.22	0.08
	Residual vector	6.87	10.35	3.19
ZY-3(S) + Pleiades-1(F)	Residual *X*	1.10	3.18	0.01
	Residual *Y*	1.10	3.17	0.001
	Residual vector	1.56	4.49	0.01
ZY-3(S) + Pleiades-1(B)	Residual *X*	1.01	2.87	0.004
	Residual *Y*	1.13	3.21	0.04
	Residual vector	1.52	4.31	0.04
ZY-3(S) + Pleiades-1(S)	Residual *X*	1.05	3.02	0.01
	Residual *Y*	1.12	3.19	0.006
	Residual vector	1.54	4.39	0.01

superior to those of the affine transformation with 2–10% improvements in the horizontal direction and 4.5–6.5% improvements in the vertical direction.

(3) In the combined adjustment, the use of a single backward-looking Pleiades-1 image produces better accuracy than the cases using the forward-looking Pleiades-1 image or both the forward-looking and backward-looking Pleiades-1 images. These differences in accuracy may relate to the imaging geometry of different image combinations.

The image residuals of CKPs were also examined to verify the performance of the combined adjustment approach. The ground coordinates of CKPs were back-projected to the stereo images using either the original RPCs or the improved RPCs from the combined adjustment. Residual vectors were drawn from the back-project points in the stereo images. Fig. 7 shows an example of the image residuals of the CKPs on the ZY-3 image, with yellow vectors representing the image residuals from the original RPCs and red for the image residuals from the improved RPCs obtained through combined adjustment of the ZY-3 imagery and the backward-looking Pleiades-1 image. Table 3 lists the detailed statistics of the image residuals from different methods for the ZY-3 image set, including the mean absolute error (MAE), maximum, and minimum. From Fig. 7 and Table 3, it can be seen that the image residuals are largely reduced after the combined adjustment of the ZY-3 imagery and the Pleiades-1 imagery. The MAE residuals are reduced from about 7 pixels before the combined adjustment to 1.5 pixels after the combined adjustment.

4.1.3. Performances of using the dominating RPCs and ridge estimation

To examine the performances of using the dominating RPCs and ridge estimation, a separate experimental analysis was carried out. Combined adjustments were conducted for the ZY-3 stereo images and Pleiades-1 stereo images, and for the SPOT-7 stereo images and Pleiades-1 stereo images, respectively, and the full set of 78 RPCs of the images were used. The combined adjustments with or without the ridge estimation were also tested. Table 4 shows the results. From Table 4 it can be seen that the obtained geo-positioning accuracy using the full set of RPCs is in the same level with those only using the dominating RPCs (refer to the corresponding results in Table 2), which demonstrates the effectiveness

Table 4
Testing results about the performances of dominating rpcs and ridge estimation.

Combinations	RPCs	Methods	Geo-positioning accuracy (RMSE in meters)		
			x	*y*	*z*
ZY-3(S) + Pleiades-1(S)	Full set of RPCs	No ridge estimation involved	No convergent solution		
ZY-3(S) + Pleiades-1(S)	Full set of RPCs	Ridge estimation involved	3.73	3.85	2.35
SPOT-7(S) + Pleiades-1(S)	Full set of RPCs	No ridge estimation involved	No convergent solution		
SPOT-7(S) + Pleiades-1(S)	Full set of RPCs	Ridge estimation involved	2.12	1.69	3.31

Fig. 8. CKPs on the ZY-3 imagery outside the overlapping region.

Table 5
Geo-positioning accuracies of ZY-3 imagery outside the overlapping region.

Combinations	Methods	Geo-positioning accuracy (RMSE in meters)		
		x	*y*	*z*
ZY-3(S)	Affine transformation (using 6 GCPs)	2.629	4.105	3.189
ZY3(S) + Pleiades-1(F)	Combined adjustment	3.129	4.352	2.954
ZY3(S) + Pleiades-1(B)	Combined adjustment	2.288	3.773	2.949
ZY3(S) + Pleiades-1(S)	Combined adjustment	2.653	4.044	2.947

of the dominating RPCs. When using the full set of RPCs, the combined adjustment cannot reach a convergent solution with no ridge estimation involved. When ridge estimation is utilized, the combined adjustment reaches a convergent solution in about 10 iterations; while only using dominating RPCs, a convergent solution can be reached in about 3 iterations. This indicates the improvements in computational efficiency by using the dominating RPCs compared to its full set.

4.1.4. Geo-positioning accuracy outside the overlapping region of the images

As the combined adjustment method corrects the dominating RPCs directly, the geo-positioning accuracy outside the overlapping regions should also be improved. To validate this aspect, the ZY-3 imagery was used for checking purposes. Sixteen CKPs distributed outside the overlapping region were selected. The distributions of these CKPs are shown in Fig. 8, and the geo-positioning accuracies determined by these CKPs are summarized in Table 5.

The results in Table 5 show that the geo-positioning accuracy of the ZY-3 imagery outside the overlapping region is generally in the same level with those within the overlapping region, slightly better in the horizontal direction and slightly worse in the vertical direction. The use of the backward-looking Pleiades-1 image produces better accuracies than those from the affine transformation using 6 GCPs in both horizontal and vertical directions. The results indi-

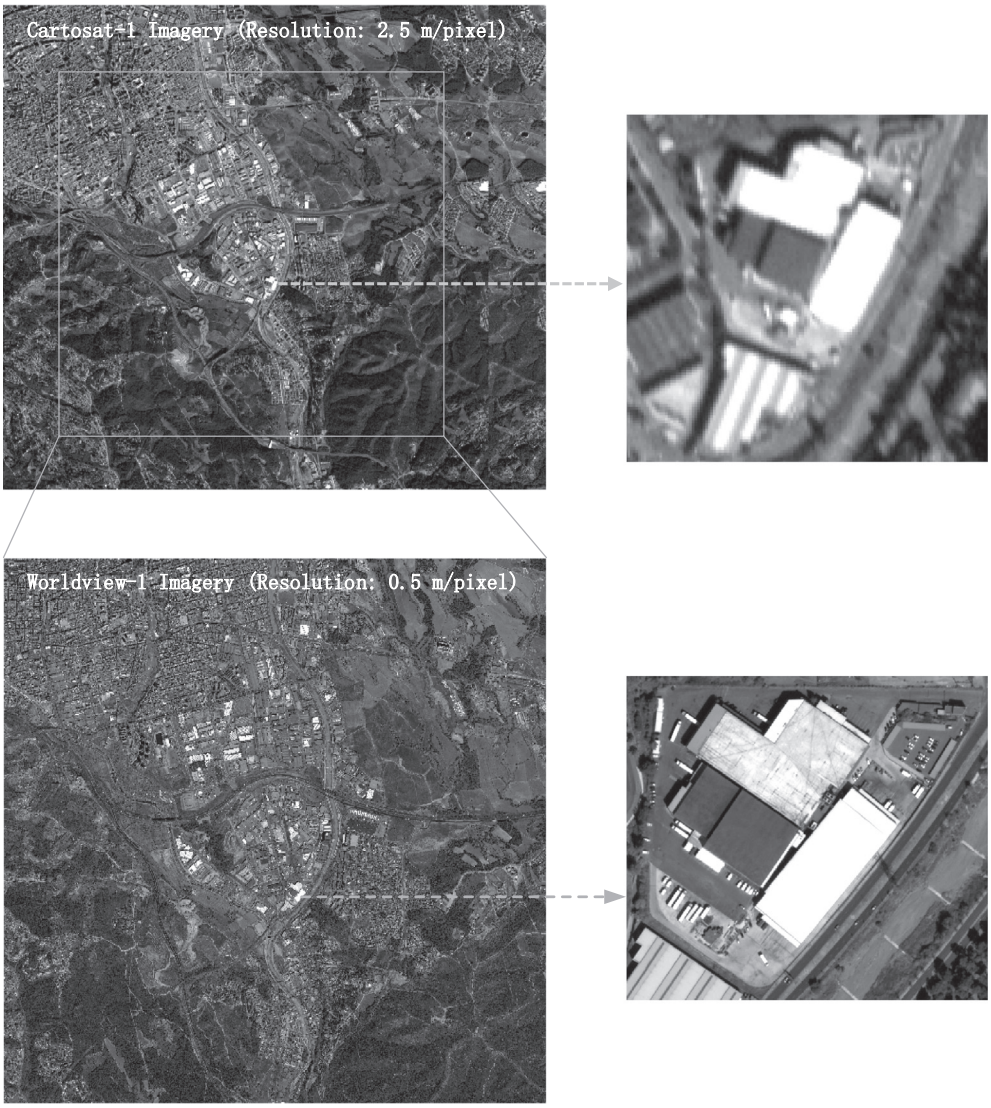

Fig. 9. The Cartosat-1 and Worldview-1 imagery in Catalonia, Spain showing different levels of coverage and resolution, with zoom-in images showing in the right.

Table 6
Geo-positioning accuracies for Worldview-1and cartosat-1 imagery from different approaches.

Combinations	Methods	Geo-positioning accuracy (RMSE in meters)			Relative improvements comparing with the results of direct space intersection	
		x	*y*	*z*	Horizontal direction (%)	Vertical direction (%)
Worldview-1(S)	Direct space intersection	1.39	0.99	0.88		
Cartosat-1(S)	Direct space intersection	2.59	2.86	4.60		
Cartosat-1(S) + Worldview-1(S)	Combined adjustment	1.59	2.36	2.48	26.25	46.09

cate that the combined adjustment approach is able to improve the geo-positioning accuracy of the entire satellite image even if the reference image only covers a small portion of the former.

4.2. Experiment using multi-resolution satellite imagery in Catalonia, Spain

4.2.1. Used data

Multi-resolution satellite images in another test site (Catalonia, Spain) have been used for validation of the proposed method. The images were downloaded from ISPRS Stereo benchmark datasets,[2] including a stereo pair of Cartosat-1 images with a resolution of 2.5 m/pixel and a stereo pair of Worldview-1 images with a resolution of 0.5 m/pixel. The DEM and orthoimages in the same area produced by airborne DMC stereo were also downloaded for comparison. Fig. 9 shows the overview of the two image sets.

In the experimental analysis, the imagery with higher resolution, i.e., the Worldview-1 imagery, was used as the reference imagery to correct the dominating RPCs of the Cartosat-1 imagery. There were 22 tie points identified on both the Cartosat-1 and the Worldview-1 stereo images. 20 CKPs were selected in the overlapping region of the two image sets from the downloaded DEM and orthoimages.

4.2.2. Performance of the combined adjustment

The results from the direct space intersection of the Cartosat-1 imagery using the original RPCs and the combined adjustment of Cartosat-1 and Worldview-1 imagery were obtained and they are presented in Table 6. The experimental results from the combined adjustment using only one Worldview-1 image were similar with those when the stereo pair of Worldview-1 images was used, therefore they are ignored here.

As can be seen from Table 6, the direct space intersection of the Cartosat-1 imagery using the original RPCs produces a horizontal accuracy of about 4 m and a vertical accuracy of 4.6 m. The use of the Worldview-1 imagery in the combined adjustment improves the geo-positioning accuracy of the Cartosat-1 imagery to about 2.85 m in horizontal direction and 2.48 m in vertical direction, indicating relative improvements of 26.25% and 46.09% in horizontal and vertical directions, respectively. The obtained results from this experiment are consistent with those from the previous experiment using the image sets in Hong Kong.

5. Conclusions and discussion

A combined adjustment method is proposed to integrate multi-source multi-resolution satellite imagery for improved geo-positioning accuracy. Based on the theoretical analysis and experimental validation, the following conclusions can be reached: The combined adjustment method is able to effectively improve the geo-positioning accuracy of lower-resolution satellite images by adding a single or a stereo pair of higher-resolution satellite images. Using a Pleiades-1 image in the combined adjustment, the geo-positioning accuracy of the ZY-3 imagery can be improved from 16 m to 5 m in the horizontal direction, and that for the SPOT-7 imagery can be improved from 6 m to 2.5 m. The accuracies in the vertical direction for the ZY-3 and SPOT-7 imagery are also improved. Similar tendency in improvements of geo-positioning accuracy can be found for the Cartosat-1 imagery through the use of the Worldview-1 imagery in the combined adjustment. The proposed combined adjustment method offers slightly better geo-positioning accuracy compared with the tradition method of bias-compensation of RPCs by means of affine transformation using GCPs.

The combined adjustment method enables the integration of multi-source multi-resolution satellite imagery for generating more precise and consistent 3D spatial information. This approach permits the full comparative and synergistic use of satellite images from different sources. It should be noted that currently, part of the procedure for selecting the tie points from images with different resolutions is done manually. Our future efforts will develop an automatic image-matching method for determining tie points from images with different resolutions, which will facilitate the fully automatic processing of the proposed approach.

[2] Available at http://www2.isprs.org/commissions/comm1/wg4/benchmark-test.html.

Acknowledgements

The authors would like to thank the Satellite Surveying and Mapping Application Center of National Administration of Surveying, Mapping and Geoinformation of China for providing the ZY-3 imagery, and the Hong Kong government's Civil Engineering and Development Department for providing the LiDAR dataset. This work was supported by a grant from the Research Grants Council of Hong Kong (Project No. PolyU 5330/12E) and a grant from the National Natural Science Foundation of China (Project No. 91338110).

References

Baltsavias, E., Pateraki, M., Zhang, L., 2001. Radiometric and geometric evaluation of Ikonos GEO images and their use for 3D building modelling. In: Proceedings of the Joint ISPRS Workshop on High Resolution Mapping from Space, Hannover, Germany, 19–21 September 2001, 21 pp. (on CD ROM).

Croft, J., 2008. Prodigious mapping capabilities, spatial resolution and geo-location ability, GeoEye's next-generation imaging satellite. Geoinformatics 4, 18–23.

Di, K., Ruijin, M., Li, R., 2003a. Geometric processing of IKONOS stereo imagery for coastal mapping applications. Photogrammetric Eng. Remote Sensing 69 (8), 873–879.

Di, K., Ma, R., Li, R., 2003b. Rational functions and potential for rigorous sensor model recovery. Photogrammetric Eng. Remote Sensing 69 (1), 33–41.

Dial, G., Grodecki, J., 2002. Block adjustment with rational polynomial camera models. In: Proceedings of ASPRS 2002 Conference, Washington, DC, pp. 22–26.

Fraser, C., 1999. Status of high-resolution satellite imaging. In: Fritsch, D., Hobbie, D. (Eds.), Proceedings of the Photogrammetric Week '99, Suttgart, Germany, 22–26 September, 1999, pp. 117–123.

Fraser, C.S., Baltsavias, E., Gruen, A., 2002. Processing of IKONOS imagery for submetre 3D positioning and building extraction. ISPRS J. Photogrammetry Remote Sensing 56 (3), 177–194.

Fraser, C.S., Dial, G., Grodecki, J., 2006. Sensor orientation via RPCs. ISPRS J. Photogrammetry Remote Sensing 60 (3), 182–194.

Fraser, C.S., Hanley, H.B., 2003. Bias compensation in rational functions for Ikonos satellite imagery. Photogrammetric Eng. Remote Sensing 69 (1), 53–57.

Fraser, C.S., Hanley, H.B., 2005. Bias-compensated RPCs for sensor orientation of high-resolution satellite imagery. Photogrammetric Eng. Remote Sensing 71 (8), 909–915.
Fraser, C.S., Ravanbakhsh, M., 2009. Georeferencing accuracy of GeoEye-1 imagery. Photogrammetric Eng. Remote Sensing 75 (6), 634–638.
Fraser, C.S., Yamakawa, T., 2004. Insights into the affine model for high-resolution satellite sensor orientation. ISPRS J. Photogrammetry Remote Sensing 5 (58), 275–288.
Glenn, N.F., Streutker, D.R., Chadwick, D.J., Thackray, G.D., Dorsch, S.J., 2006. Analysis of LiDAR-derived topographic information for characterizing and differentiating landslide morphology and activity. Geomorphology 73 (1), 131–148.
Habib, A., Shin, S.W., Kim, K., Kim, C., Bang, K., Kim, E., Lee, D., 2007. Comprehensive analysis of sensor modeling alternatives for high resolution imaging satellites. Photogrammetric Eng. Remote Sensing 73 (11), 1241–1251.
Hansen, P.C., O'Leary, D.P., 1993. The use of the L-curve in the regularization of discrete ill-posed problems. SIAM J. Sci. Comput. 14 (6), 1487–1503.
Jeong, J., Yang, C., Kim, T., 2015. Geo-positioning accuracy using multiple-satellite images: IKONOS, QuickBird, and KOMPSAT-2 stereo images. Remote Sensing 7, 4549–4564.
Kasai, M., Ikeda, M., Asahina, T., Fujisawa, K., 2009. LiDAR-derived DEM evaluation of deep-seated landslides in a steep and rocky region of Japan. Geomorphology 113 (1), 57–69.
Li, R., Deshpande, S., Niu, X., Zhou, F., Di, K., Wu, B., 2008. Geometric integration of aerial and high-resolution satellite imagery and application in shoreline mapping. Mar. Geodesy 31 (3), 143–159.
Neumaier, A., 1998. Solving ill-conditioned and singular linear systems: a tutorial on regularization. Siam Rev. 40 (3), 636–666.
Niu, X., Zhou, F., Di, K., Li, R., 2005. 3D geopositioning accuracy analysis based on integration of QuickBird and IKONOS imagery. In: Proceedings of ISPRS Hannover Workshop 2005 in High Resolution Earth Imaging for Geospatial Information, Hannover, Germany, 17–20 May 2005.
Pan, H., Zhang, G., Tang, X., Li, D., Zhu, X., Zhou, P., Jiang, Y., 2013. Basic products of the ZiYuan-3 satellite and accuracy evaluation. Photogrammetric Eng. Remote Sensing 79 (12), 1131–1145.
Poli, D., Remondino, F., Angiuli, E., Agugiaro, G., 2013. Evaluation of Pleiades-1a triplet on Trento testfield. Int. Arch. Photogrammetry, Remote Sensing Spatial Inf. Sci. 40, 287–292.
Qiao, G., Wang, W., Wu, B., Liu, C., Li, R., 2010. Assessment of geo-positioning capability of high resolution satellite imagery for densely populated high buildings in metropolitan areas. Photogrammetric Eng. Remote Sensing 76 (8), 923–934.
Tao, C.V., Hu, Y., 2001. A comprehensive study of the rational function model for photogrammetric processing. Photogrammetric Eng. Remote Sensing 67 (12), 1347–1358.
Tong, X., Liu, S., Weng, Q., 2010a. Bias-corrected rational polynomial coefficients for high accuracy geo-positioning of QuickBird stereo imagery. ISPRS J. Photogrammetry Remote Sensing 65 (2), 218–226.
Tong, X., Liu, S., Xie, H., Wang, W., Chen, P., Bao, F., 2010b. Geometric integration of aerial and QuickBird imagery for high accuracy geopositioning and mapping application: a case study in Shanghai. Mar. Geodesy 33 (4), 437–449.
Toutin, T., 2006. Comparison of 3D physical and empirical models for generating DSMs from stereo HR images. Photogrammetric Eng. Remote Sensing 72 (5), 597–604.
Wang, Z., Ou, J., 2004. Determining the ridge parameter in a ridge estimation using L-curve method. Geomatics Inf. Sci. Wuhan Univ. 29 (3), 235–238.
Wang, J., Di, K., Li, R., 2005. Evaluation and improvement of geopositioning accuracy of IKONOS stereo imagery. J. Surveying Eng. 131 (2), 35–42.
Wang, T., Zhang, G., Li, D., Tang, X., Jiang, Y., Pan, H., Zhu, X., 2014. Planar block adjustment and orthorectification of ZY-3 satellite images. Photogrammetric Eng. Remote Sensing 80 (6), 559–570.
Wu, B., Zhang, Y., Zhu, Q., 2011a. A triangulation-based hierarchical image matching method for wide-baseline images. Photogrammetric Eng. Remote Sensing 77 (7), 695–708.
Wu, B., Guo, J., Zhang, Y., King, B.A., Li, Z., Chen, Y., 2011b. Integration of Chang'E-1 imagery and laser altimeter data for precision lunar topographic modeling. IEEE Trans. Geosci. Remote Sensing 49 (12), 4889–4903.
Wu, B., Zhang, Y., Zhu, Q., 2012. Integrated point and edge matching on poor textural images constrained by self-adaptive triangulations. ISPRS J. Photogrammetry Remote Sensing 68 (2012), 40–55.
Wu, B., Hu, H., Guo, J., 2014. Integration of Chang'E-2 imagery and LRO laser altimeter data with a combined block adjustment for precision lunar topographic modeling. Earth Planet. Sci. Lett. 391, 1–15.
Wu, B., Tang, S., Zhu, Q., Tong, K., Hu, H., Li, G., 2015. Geometric integration of high-resolution satellite imagery and airborne LiDAR data for improved geopositioning accuracy in metropolitan areas. ISPRS J. Photogrammetry Remote Sensing 109, 139–151.
Yoon, J., Shan, J., 2005. Combined adjustment of MOC stereo imagery and MOLA altimetry data. Photogrammetric Eng. Remote Sensing 71 (10), 1179–1186.
Yuan, X., Lin, X., 2008. A method for solving rational polynomial coefficients based on ridge estimation. Geomatics Inf. Sci. Wuhan Univ. 33 (11), 1130–1133.
Zhu, Q., Wu, B., Wan, N., 2007. A filtering strategy for interest point detecting to improve repeatability and information content. Photogrammetric Eng. Remote Sensing 73 (5), 547–553.